Available online at www.sciencedirect.com
ScienceDirect
Journal of Solid State Chemistry 180 (2007) 186–190
JOURNAL OF SOLID STATE CHEMISTRY
www.elsevier.com/locate/jssc

Bridgman crystal growth of $Yb_2Ru_3Ge_4$—A ternary germanide with a three-dimensional network of condensed distorted $RuGe_5$ and $RuGe_6$ units

Falko M. Schappacher[a], Kenichi Katoh[b], Rainer Pöttgen[a,*]

[a]*Institut für Anorganische und Analytische Chemie, Universität Münster, Corrensstrasse 30, 48149 Münster, Germany*
[b]*Department of Applied Physics, National Defense Academy, Hashirimizu 1-10-20 Yokosuka, 239-8686, Japan*

Received 5 September 2006; received in revised form 5 October 2006; accepted 9 October 2006
Available online 13 October 2006

Abstract

The germanide $Yb_2Ru_3Ge_4$ was synthesized from the elements using the Bridgman crystal growth technique. The monoclinic $Hf_2Ru_3Si_4$ type structure was investigated by X-ray powder and single crystal diffraction: $C2/c$, $Z = 8$, $a = 1993.0(3)$ pm, $b = 550.69(8)$ pm, $c = 1388.0(2)$ pm, $\beta = 128.383(9)^\circ$, $wR_2 = 0.0569$, 2047 F^2 values, and 84 variables. $Yb_2Ru_3Ge_4$ contains two crystallographically independent ytterbium sites with coordination numbers of 18 and 17 for Yb1 and Yb2, respectively. Each ytterbium atom has three ytterbium neighbors at Yb–Yb distances ranging from 345 to 368 pm. The shortest interatomic distances occur for the Ru–Ge contacts. The three crystallographically independent ruthenium sites have between five and six germanium neighbors in distorted trigonal bipyramidal ($Ru1Ge_5$) or octahedral ($Ru2Ge_6$ and $Ru3Ge_6$) coordination at Ru–Ge distances ranging from 245 to 279 pm. The Ru2 atoms form zig-zag chains running parallel to the *b*-axis at Ru2–Ru2 of 284 pm. The $RuGe_5$ and $RuGe_6$ units are condensed via common edges and faces leading to a complex three-dimensional $[Ru_3Ge_4]$ network.

Keywords: Germanide; Crystal growth; Intermetallics; Crystal chemistry

1. Introduction

Intermetallic $Yb_xT_yX_z$ compounds (T = late transition metal; X = element of the 3rd, 4th, or 5th main group) are interesting candidates when searching for intermediate valence materials, since ytterbium can occur in the diamagnetic divalent ([Xe]$4f^{14}$) or paramagnetic trivalent ([Xe]$4f^{13}$) oxidation state. Especially the trivalent ytterbium compounds are interesting for comparison with related cerium intermetallics, since they exhibit the f-hole analogue of [Xe]$4f^1$ cerium. In principle, the Kondo effect should be symmetrical between electrons and holes and furthermore, also heavy fermion behavior should occur for ytterbium intermetallics [1, 2].

A severe problem for the synthesis of intermetallic ytterbium compounds is the comparatively low boiling temperature of 1466 K [3]. Sample preparation in quasi-open systems like an arc melting furnace results in significant evaporations and irreversible change of the starting composition. Thus, one needs synthesis in closed reaction containers. This is especially important when elements with significantly different melting and boiling temperatures should be reacted. We have recently used a *Bridgman* crystal growth procedure in sealed tungsten crucibles for the preparation of ytterbium-transition metal-germanides [4–7, and ref. therein].

So far, only the Yb–*T*–Ge systems with the 3*d* transition metals and palladium have been investigated in detail [8,9, and ref. therein], however, not all structures of these germanides have been determined. We have started a more systematic study of the Yb–*T*–Ge systems with respect to the 4*d* and 5*d* transition metals. The crystal growth procedure and the structure refinement of the new monoclinic germanide $Yb_2Ru_3Ge_4$ are described herein.

*Corresponding author. Fax: +49 251 83 36002.
E-mail addresses: katok@nda.ac.jp (K. Katoh), pottgen@uni-muenster.de (R. Pöttgen).

0022-4596/$ - see front matter © 2006 Elsevier Inc. All rights reserved.
doi:10.1016/j.jssc.2006.10.008

2. Experimental

2.1. Synthesis

Starting materials for the preparation of $Yb_2Ru_3Ge_4$ were ingots of ytterbium (>99.9%), ruthenium powder (>99.9%), and germanium lumps (>99.99%). In a first step a binary alloy of composition Ru_3Ge_5 was prepared by arc-melting under an atmosphere of purified argon. Then, ytterbium pieces and the Ru_3Ge_5 alloy (2:1 ratio) were sealed in a tungsten crucible under vacuum using an electron beam welder. The use of a precursor alloy ensures complete reaction with the ytterbium pieces. The crucible was subsequently heated up to 1653 K in a Bridgman furnace and kept at that temperature for one hour. Finally the crucible was pulled down at a rate of 2 mm/h. A lump of cube-shaped $Yb_2Ru_3Ge_4$ crystals (~1 mm edge length) was obtained and the crystals could easily be separated from the tungsten crucible. The compact and polycrystalline $Yb_2Ru_3Ge_4$ samples are stable in moist air over months. Single crystals exhibit metallic lustre. Polycrystalline $Yb_2Ru_3Ge_4$ can also be obtained from a direct reaction of the elements in a sealed tantalum tube.

2.2. X-ray powder data

The sample was characterized through a Guinier powder pattern using Cu$K\alpha_1$ radiation and α-quartz ($a = 491.30$ pm, $c = 540.46$ pm) as internal standard. The Guinier camera was equipped with an imaging plate system (Fujifilm, BAS-1800). The monoclinic lattice parameters (Table 1) were refined by least-squares calculations using the WinXPow software supplied by Stoe. To ensure proper indexing, the experimental pattern was compared to a calculated one [10], taking the atomic sites derived from the single crystal data. The lattice parameters determined on the single-crystal diffractometer ($a = 1993.6(4)$ pm, $b = 550.7(1)$ pm, $c = 1388.7(3)$ pm, $\beta = 128.40(3)^\circ$) were in good agreement with the powder data.

2.3. Single crystal X-ray diffraction

Irregularly shaped crystals of $Yb_2Ru_3Ge_4$ were selected from a crushed part of the larger crystal obtained by the Bridgman technique. These crystals were glued to small quartz fibres using bees wax and then first checked by Laue photographs on a Buerger camera, equipped with the same Fujifilm, BAS-1800 imaging plate technique. A good quality crystal was then used for the intensity data collection on a Stoe IPDS II diffractometer (graphite monochromatized Mo$K\alpha$ radiation; oscillation mode). A numerical absorption correction was applied to the data set. All relevant crystallographic data for the data collection and evaluation are listed in Table 1.

Table 1
Crystal data and structure refinement for $Yb_2Ru_3Ge_4$

Empirical formula	$Yb_2Ru_3Ge_4$
Molar mass	939.65 g/mol
Unit cell dimensions	$a = 1993.0(3)$ pm
(Guinier powder data)	$b = 550.69(8)$ pm
	$c = 1388.0(2)$ pm
	$\beta = 128.383(9)^\circ$
	$V = 1.1941$ nm^3
Space group, Z	$C2/c$; $Z = 8$
Structure type	$Hf_2Ru_3Si_4$
Pearson symbol	mC72
Calculated density	10.45 g/cm^3
Crystal size	$20 \times 30 \times 150$ μm^3
Detector distance	80 mm
Exposure time	5 min
ω range; increment	0–180°, 1.0°
Integration parameters A, B, EMS	15.2, 4.0, 0.028
Transm. ratio (max/min)	3.71
Absorption coefficient	58.0 mm^{-1}
$F(000)$	3200
θ range	2–32°
Range in hkl	–29/+25, ±8, ±20
Total no. reflections	6830
Independent reflections	2047 ($R_{int} = 0.0607$)
Reflections with $I > 2\sigma(I)$	1469 ($R_\sigma = 0.0667$)
Data/parameters	2047/84
Goodness-of-fit on F^2	0.833
Weighting scheme[a]	$a = 0.0258$; $b = 0$
Final R indices [$I > 2\sigma(I)$]	$R1 = 0.0261$; w$R2 = 0.0549$
R indices (all data)	$R1 = 0.0422$; w$R2 = 0.0569$
Extinction coefficient	0.00203(4)
Largest diff. peak and hole	2.39/–3.67 e/Å^3

[a]Weight $= 1/[\sigma^2(F_o^2) + (aP)^2 + bP]$ where $P = 1/3 \max(0, F_o^2) + 2/3\, F_c^2$.

2.4. Scanning electron microscopy

The single crystals investigated on the diffractometer and the bulk samples were analysed using a LEICA 420 I scanning electron microscope with YbF_3, Ru, and Ge as standards. No impurity elements heavier than sodium were observed. The compositions determined by EDX (24±2 at% Yb : 33±2 at% Ru : 43±2 at% Ge) are in good agreement with the ideal composition, i.e. 22.2:33.3:44.4. The standard uncertainties account for the analyses at various points.

3. Results and discussion

3.1. Structure refinement

Careful analyses of the IDPS data revealed a monoclinic C-centered unit cell and the observed systematic extinctions were compatible with space groups Cc and $C2/c$, of which the centrosymmetric group was found to be correct during structure refinement. The starting atomic parameters were determined by an automatic interpretation of direct methods with SHELXS-97 [11] and the structure was refined with anisotropic displacement parameters for all atoms with SHELXL-97 (full-matrix least-squares on F_o^2) [12]. Inspection of the Pearson Handbook [13] for the

Table 2
Atomic coordinates and anisotropic displacement parameters (pm^2) of $Yb_2Ru_3Ge_4$

Atom	Wyck.	x	Y	z	U_{11}	U_{22}	U_{33}	U_{23}	U_{13}	U_{12}	U_{eq}
Yb_1	8*f*	0.16304(2)	0.12222(8)	0.35846(4)	30(1)	27(2)	35(2)	–6(2)	27(1)	–3(1)	26(1)
Yb_2	8*f*	0.43014(2)	0.13509(8)	0.35799(4)	47(2)	24(2)	45(2)	–3(2)	40(1)	–4(1)	31(1)
Ru_1	8*f*	0.01882(4)	0.1236(2)	0.41335(7)	22(3)	33(3)	20(3)	1(3)	18(2)	–1(3)	21(1)
Ru_2	8*f*	0.23980(4)	0.4016(1)	0.21913(7)	28(3)	10(3)	21(3)	–2(3)	17(2)	–4(2)	19(1)
Ru_3	8*f*	0.37701(4)	0.1361(2)	0.06647(7)	34(3)	26(3)	29(3)	2(3)	23(2)	4(3)	27(1)
Ge_1	8*f*	0.11210(5)	0.1445(2)	0.10490(9)	29(4)	34(4)	35(4)	–18(4)	26(3)	–10(4)	29(2)
Ge_2	8*f*	0.26581(6)	0.1205(2)	0.1050(1)	41(4)	25(4)	48(4)	–9(4)	38(3)	–2(4)	31(2)
Ge_3	8*f*	0.32902(6)	0.2356(2)	0.4339(1)	30(4)	17(4)	26(4)	–3(4)	20(3)	–7(3)	22(2)
Ge_4	4*e*	0	0.3829(3)	1/4	37(5)	23(6)	29(6)	0	29(5)	0	24(2)
Ge_5	4*e*	0	0.8725(3)	1/4	35(5)	21(6)	21(6)	0	23(5)	0	21(2)

The anisotropic displacement factor exponent takes the form: $-2\pi^2[(ha^*)^2U_{11}+,\cdots,+2hka^*b^*U_{12}]$. U_{eq} is defined as one third of the trace of the orthogonalized U_{ij} tensor.

Pearson code mC72 then readily revealed isotypism with $Hf_2Ru_3Si_4$ [14,15]. Consequently, in the final cycles, the $Yb_2Ru_3Ge_4$ structure was refined with the setting of $Hf_2Ru_3Si_4$. The occupancy parameters have been refined in a separate series of least-squares cycles. All sites were fully occupied within three standard uncertainties and in the final cycles, the ideal occupancy parameters were assumed again. A final difference Fourier synthesis revealed no significant residual peaks. The refinement then converged to the residuals listed in Table 1 and the atomic parameters and interatomic distances listed in Tables 2 and 3. Further data on the structure refinement are available.[1]

3.2. Crystal chemistry

New germanide $Yb_2Ru_3Ge_4$ was synthesized via a Bridgman crystal growth technique. $Yb_2Ru_3Ge_4$ is isotypic with $Hf_2Ru_3Si_4$ [14,15]. So far, only $Zr_2Ru_3Si_4$ [15] crystallizes with this peculiar monoclinic structure type, and $Sc_3Re_2Si_4$ can be considered as a site occupancy variant of $Hf_2Ru_3Si_4$ [14]. The $Sc_3Re_2Si_4$ and $Hf_2Ru_3Si_4$ structures belong to a larger family of intermetallic structure types that can be constructed from infinite antiprism and octahedron columns. Chabot and Parthé effectively used this classification scheme to predict the structure of $Sc_3Re_2Si_4$ [14].

A view of the complex $Yb_2Ru_3Ge_4$ structure is presented in Fig. 1. The shortest interatomic distances occur for the Ru–Ge contacts. The Ru–Ge distances cover the range from 245 to 279 pm, close to the sum of the covalent radii of 246 pm [3]. We can thus assume significant Ru–Ge bonding. The $[Ru_3Ge_4]$ network is three-dimensional and leaves voids that are filled by the ytterbium atoms.

The three crystallographically independent ruthenium atoms have different germanium coordination, i.e. a distorted trigonal bipyramid for $Ru1Ge_5$ and distorted octahedra for $Ru2Ge_6$ and $Ru3Ge_6$. These polyhedra are condensed, building the network shown in Fig. 2. A cutout of this network is presented in Fig. 3. The $Ru2Ge_6$ octahedra are *trans* face-shared and we observed Ru2–Ru2 distances of 284 pm between the octahedra, leading to zig-zag chains that run parallel to the monoclinic axis. The Ru2–Ru2 distances are only slightly longer than the average Ru–Ru distance of 268 pm in *hcp* ruthenium [16]. These Ru–Ru distances compare well with the Ru_4 cluster units in $CeRu_4Sn_6$ [17] and $GdRu_4Sn_6$ [18]. The $Ru3Ge_6$ octahedra are condensed to the infinite chain of $Ru2Ge_6$ octahedra via common, distorted triangular faces. The distorted trigonal bipyramids $Ru1Ge_5$ share common edges with the $Ru2Ge_6$ and $Ru3Ge_6$ units (Fig. 3).

The various binary and ternary ruthenium germanides show peculiar $RuGe_x$ ($x = 4$–7) coordination. The structure of Ru_2Ge_3 contains three crystallographically independent ruthenium sites $Ru1Ge_7$, $Ru2Ge_4$, and $Ru3Ge_6$ with Ru–Ge distances ranging from 238 to 266 pm [19], similar to $Yb_2Ru_3Ge_4$. The Ru2 atoms have four further germanium neighbors at much longer Ru–Ge distances of 276 and 292 pm, completing the coordination sphere. The Ru–Ru distances between the $RuGe_x$ units in Ru_2Ge_3 of 299 and 307 pm are much longer than in the $[Ru_3Ge_4]$ network of $Yb_2Ru_3Ge_4$.

If the structures have a higher rare earth metal content, the rare earth atoms can transfer more electron density towards the ruthenium and germanium atoms and consequently the dimensionality of the $[Ru_yGe_z]$ networks and/or the coordination number decrease. The structures of HoRuGe, $Ho_3Ru_2Ge_3$ [20], and Tb_2RuGe_2 [21] have distorted $RuGe_4$ tetrahedra as structural building units with Ru–Ge distances ranging from 244 to 267 pm. In HoRuGe the tetrahedra share common edges and corners leading to a three-dimensional network, while the network of edge- and corner-sharing tetrahedra in $Ho_3Ru_2Ge_3$ [20] is two dimensional. In Tb_2RuGe_2 [21], the $RuGe_4$ tetrahedra form isolated chains via corner-sharing.

Finally we draw back to the ytterbium coordination in the $Yb_2Ru_3Ge_4$ structure. Both crystallographically

[1]Details may be obtained from: Fachinformationszentrum Karlsruhe, D-76344 Eggenstein-Leopoldshafen (Germany), by quoting the Registry No. CSD-416964.

Table 3
Interatomic distances (pm), calculated with the lattice parameters taken from X-ray powder data of $Yb_2Ru_3Ge_4$

Yb_1:1	Ge_3	285.1	Ru_1:1	Ge_1	246.3	Ru_3:1	Ge_3	251.1	Ge_3:1	Ru_2	248.1
Yb_1:1	Ge_3	289.4	Ru_1:1	Ge_5	247.7	Ru_3:1	Ge_5	253.8	Ge_3:1	Ru_2	251.1
Yb_1:1	Ge_5	294.0	Ru_1:1	Ge_4	250.3	Ru_3:1	Ge_2	258.4	Ge_3:1	Ru_3	251.1
Yb_1:1	Ge_4	296.8	Ru_1:1	Ge_3	251.2	Ru_3:1	Ge_4	258.6	Ge_3:1	Ru_1	251.2
Yb_1:1	Ge_2	298.4	Ru_1:1	Ge_1	256.3	Ru_3:1	Ge_2	267.4	Ge_3:1	Ge_2	266.3
Yb_1:1	Ru_2	299.6	Ru_1:1	Yb_2	297.7	Ru_3:1	Ge_1	279.4	Ge_3:1	Ge_1	274.3
Yb_1:1	Ge_2	299.8	Ru_1:1	Yb_2	304.4	Ru_3:1	Ru_2	311.7	Ge_3:1	Yb_2	284.9
Yb_1:1	Ge_1	299.9	Ru_1:1	Yb_2	315.6	Ru_3:1	Yb_1	315.0	Ge_3:1	Yb_1	285.1
Yb_1:1	Ge_2	300.2	Ru_1:1	Yb_1	322.3	Ru_3:1	Yb_1	328.1	Ge_3:1	Yb_1	289.4
Yb_1:1	Ru_3	315.0	Ru_1:1	Ru_1	323.1	Ru_3:1	Yb_2	329.7	Ge_4:2	Ru_1	250.3
Yb_1:1	Ru_1	322.3	Ru_1:1	Ru_3	329.7	Ru_3:1	Ru_1	329.7	Ge_4:2	Ru_3	258.6
Yb_1:1	Ru_3	328.1	Ru_1:1	Yb_1	340.0	Ru_3:1	Ru_1	341.1	Ge_4:1	Ge_5	269.7
Yb_1:1	Ru_1	340.0	Ru_1:1	Ru_3	341.1	Ru_3:1	Yb_2	348.9	Ge_4:1	Ge_5	281.0
Yb_1:1	Ru_2	348.2	Ru_2:1	Ge_1	244.6	Ru_3:1	Yb_1	364.1	Ge_4:2	Yb_2	295.1
Yb_1:1	Yb_1	353.9	Ru_2:1	Ge_3	248.1	Ge_1:1	Ru_2	244.6	Ge_4:2	Yb_1	296.8
Yb_1:1	Yb_2	357.0	Ru_2:1	Ge_2	248.9	Ge_1:1	Ru_1	246.3	Ge_5:2	Ru_1	247.7
Yb_1:1	Ru_3	364.1	Ru_2:1	Ge_3	251.1	Ge_1:1	Ru_1	256.3	Ge_5:2	Ru_3	253.8
Yb_1:1	Yb_2	367.7	Ru_2:1	Ge_1	274.1	Ge_1:1	Ru_2	274.1	Ge_5:1	Ge_4	269.7
Yb_2:1	Ge_3	284.9	Ru_2:1	Ge_2	278.6	Ge_1:1	Ge_3	274.3	Ge_5:1	Ge_4	281.0
Yb_2:1	Ge_5	291.3	Ru_2:2	Ru_2	283.7	Ge_1:1	Ru_3	279.4	Ge_5:2	Yb_2	291.3
Yb_2:1	Ge_4	295.1	Ru_2:1	Yb_1	299.6	Ge_1:1	Yb_2	296.8	Ge_5:2	Yb_1	293.9
Yb_2:1	Ge_2	296.3	Ru_2:1	Ru_3	311.7	Ge_1:1	Yb_1	299.9			
Yb_2:1	Ge_1	296.8	Ru_2:1	Yb_2	312.5	Ge_1:1	Yb_2	306.3			
Yb_2:1	Ru_1	297.7	Ru_2:1	Yb_2	334.4	Ge_1:1	Ge_2	306.6			
Yb_2:1	Ru_1	304.4	Ru_2:1	Yb_1	348.2	Ge_1:1	Yb_2	330.7			
Yb_2:1	Ge_1	306.3				Ge_2:1	Ru_2	248.9			
Yb_2:1	Ru_2	312.5				Ge_2:1	Ru_3	258.4			
Yb_2:1	Ru_1	315.7				Ge_2:1	Ge_3	266.3			
Yb_2:1	Ru_3	329.7				Ge_2:1	Ru_3	267.4			
Yb_2:1	Ge_1	330.7				Ge_2:1	Ru_2	278.6			
Yb_2:1	Ru_2	334.4				Ge_2:1	Ge_2	294.1			
Yb_2:1	Yb_2	344.6				Ge_2:1	Yb_2	296.3			
Yb_2:1	Ru_3	348.9				Ge_2:1	Yb_1	298.4			
Yb_2:1	Yb_1	357.0				Ge_2:1	Yb_1	299.8			
Yb_2:1	Yb_1	367.7				Ge_2:1	Yb_1	300.2			

All distances within the first coordination spheres are listed. Standard deviations are equal or less than 0.2 pm.

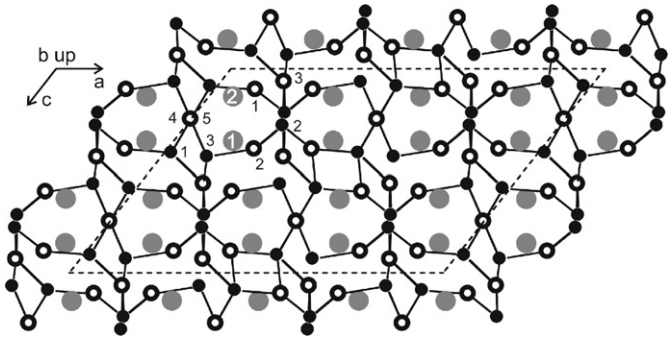

Fig. 1. View of the $Yb_2Ru_3Ge_4$ structure along the monoclinic axis. Ytterbium, ruthenium, and germanium atoms are drawn as medium grey, black filled, and open circles, respectively. The three-dimensional $[Ru_3Ge_4]$ network is emphasized. Atom designations are given in the upper left-hand part. The Ge4 and Ge5 positions superimpose (see Table 2).

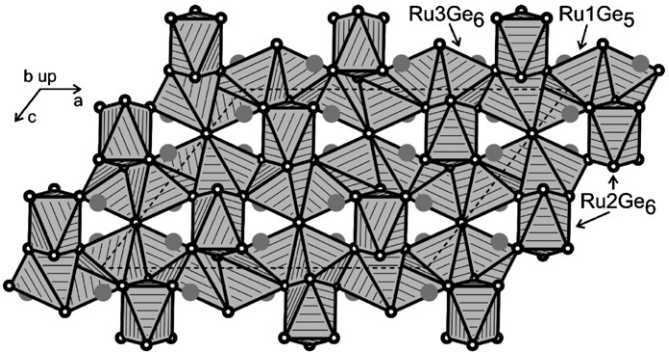

Fig. 2. View of the $Yb_2Ru_3Ge_4$ structure along the monoclinic axis. The condensed distorted trigonal bipyramidal $Ru1Ge_5$ and octahedral $Ru2Ge_6$ and $Ru3Ge_6$ units are emphasized. The ytterbium atoms fill voids within this complex network.

independent ytterbium atoms have site symmetry 1. The corresponding coordination polyhedra (coordination number 18 for Yb1 and 17 for Yb2) are presented in Fig. 4. Both polyhedra are significantly distorted, however, fragments resemble the well known Frank–Kasper polyhedra [22,23]. Both ytterbium sites show similar Yb–Ge, Yb–Ru,

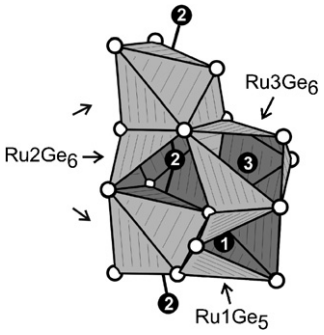

Fig. 3. Cutout of the $Yb_2Ru_3Ge_4$ structure. The zig-zag chains of the Ru2 atoms run parallel to the monoclinic axis. Each ruthenium atoms has octahedral germanium coordination. The distorted $Ru3Ge_6$ octahedra are condensed to the $Ru2Ge_6$ octahedra via common faces, while the $Ru1Ge_5$ trigonal bipyramids share common edges with the $Ru2Ge_6$ and $Ru3Ge_6$ polyhedra. For details see text.

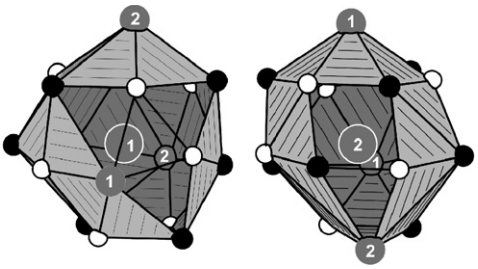

Fig. 4. Coordination polyhedra of the Yb1 and Yb2 sites in $Yb_2Ru_3Ge_4$. Ytterbium, ruthenium, and germanium atoms are drawn as medium grey, black filled, and open circles, respectively.

and Yb–Yb distances. The Yb–Ge and Yb–Ru distances of $Yb_2Ru_3Ge_4$ compare well with the Yb1–Ge and Yb1–Pd distances in $Yb_3Pd_4Ge_4$ [24], while the Yb2–Ge and Yb2–Pd distances in the latter germanide are significantly larger. Already from the course of the interatomic distances one can assume that the ytterbium atoms in $Yb_2Ru_3Ge_4$ are in a trivalent oxidation state. A detailed study on the physical properties of $Yb_2Ru_3Ge_4$ will be communicated in a forthcoming paper [25].

Acknowledgments

We are grateful to Dr. T. Nilges and Dr. R.-D. Hoffmann for the intensity data collection. This work was supported by the Deutsche Forschungsgemeinschaft.

References

[1] Z. Fisk, M.B. Maple, J. Alloys Compd. 183 (1992) 303.
[2] R. Pöttgen, D. Johrendt, D. Kußmann, in: K.A. Gschneidner Jr., L. Eyring, G. Lander (Eds.), Handbook on the Physics and Chemistry of Rare Earths, vol. 32, Elsevier Science B.V., UK, 2001 (Chapter 207).
[3] J. Emsley, The Elements, Oxford University Press, Oxford, 1999.
[4] B. Heying, K. Katoh, Y. Niide, A. Ochiai, R. Pöttgen, Z. Anorg. Allg. Chem. 630 (2004) 1423.
[5] K. Katoh, H. Abe, D. Negishi, G. Terui, Y. Niide, A. Ochiai, J. Magn. Magn. Mater. 279 (2004) 118.
[6] B. Heying, U.Ch. Rodewald, R. Pöttgen, K. Katoh, Y. Niide, A. Ochiai, Monatsh. Chem. 136 (2005) 655.
[7] K. Katoh, T. Tsutsumi, K. Yamada, G. Terui, Y. Niide, A. Ochiai, Physica B: Condens. Matter 373 (2006) 111.
[8] P.S. Salamakha, O.L. Sologub, O.I. Bodak, in: K.A. Gschneidner Jr., L. Eyring (Eds.), Handbook on the Physics and Chemistry of Rare Earths, vol. 27, Elsevier, Amsterdam, 1999 (Chapter 173).
[9] P.S. Salamakha, in: K.A. Gschneidner Jr., L. Eyring (Eds.), Handbook on the Physics and Chemistry of Rare Earths, vol. 27, Elsevier, Amsterdam, 1999 (Chapter 174).
[10] K. Yvon, W. Jeitschko, E. Parthé, J. Appl. Crystallogr. 10 (1977) 73.
[11] G.M. Sheldrick, SHELXS-97, Program for the Solution of Crystal Structures, University of Göttingen, Germany, 1997.
[12] G.M. Sheldrick, SHELXL-97, Program for Crystal Structure Refinement, University of Göttingen, Germany, 1997.
[13] P. Villars, L.D. Calvert, Pearson's Handbook of Crystallographic Data for Intermetallic Phases, second ed. American Society for Metals, Materials Park, OH 44073 (1991); and desk edition (1997).
[14] B. Chabot, E. Parthé, Acta Crystallogr. 41B (1985) 213.
[15] B. Chabot, E. Parthé, H.F. Braun, Acta Crystallogr. 41B (1985) 1148.
[16] J. Donohue, The Structures of the Elements, Wiley, New York, 1974.
[17] R. Pöttgen, R.-D. Hoffmann, E.V. Sampathkumaran, I. Das, B.D. Mosel, R. Müllmann, J. Solid State Chem. 134 (1997) 326.
[18] M.F. Zumdick, R. Pöttgen, Z. Naturforsch. 54b (1999) 863.
[19] D.J. Poutcharovsky, K. Yvon, E. Parthé, J. Less-Common Met. 40 (1975) 139.
[20] O.L. Sologub, Yu.M. Prots', P.S. Salamakha, O.I. Bodak, J. Alloys Compd. 209 (1994) 107.
[21] P. Boulet, F. Weitzer, K. Hiebl, H. Noël, J. Alloys Compd. 292 (2000) 302.
[22] F.C. Frank, J.S. Kasper, Acta Crystallogr 11 (1958) 184.
[23] F.C. Frank, J.S. Kasper, Acta Crystallogr. 12 (1959) 483.
[24] D. Niepmann, Yu.M. Prots', R. Pöttgen, W. Jeitschko, J. Solid State Chem. 154 (2000) 329.
[25] K. Katoh, unpublished results.